

Supplement To: Search for Tensor, Vector, and Scalar Polarizations in the Stochastic Gravitational-Wave Background

B. P. Abbott *et al.* (LIGO Scientific Collaboration & Virgo Collaboration)

This document contains additional information and results supplemental to the material presented in Ref. [1]. In particular, we illustrate the contributions of different frequency bands to Advanced LIGO’s stochastic search sensitivity, further describe the hypothesis testing procedure used in Ref. [1], and discuss our treatment of calibration uncertainties. Finally, we show complete parameter estimation results under a variety of hypotheses for the polarization content of the stochastic gravitational-wave background.

Sensitive Frequency Bands

Although the stochastic search for non-standard polarizations utilizes the full 20-1726 Hz frequency band, different frequency sub-bands contribute variously to our overall search sensitivity. To illustrate this, we can investigate the contribution from each frequency bin to a background’s optimal signal-to-noise ratio (SNR), given by [2]

$$\text{SNR}^2 = \frac{3H_0^2}{10\pi^2} 2T \int_0^\infty \frac{[\sum_A \gamma_A(f) \Omega^A(f)]^2}{f^6 P_1(f) P_2(f)} df. \quad (\text{A1})$$

Up to additive constants, SNR and $\mathcal{O}_N^{\text{SIG}}$ are related by $\ln \mathcal{O}_N^{\text{SIG}} \sim \text{SNR}^2/2$.

Using the measured O1 search sensitivity, Fig. 1 illustrates the cumulative fraction of the squared-SNR of several representative hypothetical backgrounds, obtained by integrating Eq. (A1) from 20 Hz up to a cutoff frequency f . Results are shown for purely tensor- (blue), vector- (red), and scalar-polarized (green) backgrounds, with spectral indices $\alpha = -8, 0, \text{ and } 8$.

As seen in Fig. 1, the most sensitive frequency band for a given background is highly dependent on the background’s spectral index. For steeply negatively-sloped backgrounds ($\alpha = -8$), the majority of the measured SNR is obtained at very low frequencies between $\sim 20 - 30$ Hz. Meanwhile, the $\sim 20 - 100$ Hz band is most sensitive to flat backgrounds, and high frequencies above ~ 700 Hz are most sensitive to steeply positively-sloped backgrounds. Although trends are generally independent of polarization, Fig. 1 does show somewhat different behaviors for tensor, vector, and scalar modes. These differences are due to the different overlap reduction functions for each polarization sector.

Model Construction

Here, we briefly summarize the construction of our Signal, Gaussian noise, Non-standard polarization, and Tensor-polarization hypotheses; see Ref. [3] for further details.

Gaussian noise: We assume that no signal is present and the observed cross-power $\hat{C}(f)$ is Gaussian distributed about zero with variance given by Eqs. (9) and (12) of Ref. [1]. Although Advanced LIGO instrumental noise is neither stationary nor Gaussian, searches for the stochastic background

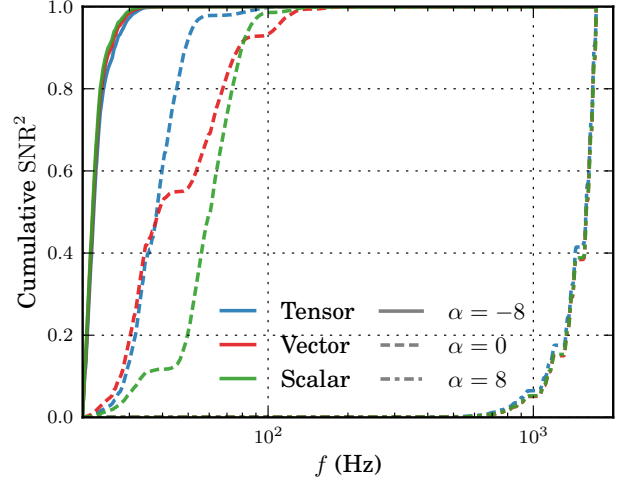


FIG. 1. Cumulative squared signal-to-noise ratios as a function of frequency for hypothetical backgrounds of tensor (blue), vector (red), scalar (green) polarizations with spectral indices $\alpha = -8, 0, \text{ and } 8$ (solid, dashed, and dot-dashed, respectively). The three $\alpha = -8$ curves lie nearly on top of one another, as do the three $\alpha = 8$ curves. The Advanced LIGO network is most sensitive to negatively-sloped backgrounds at low frequencies, while high frequencies contribute the most sensitively to positively-sloped backgrounds.

are nonetheless well-described by Gaussian statistics due to the large number of time-segments combined to form the final cross-power spectrum $\hat{C}(f)$ [4].

Signal: The Signal hypothesis is the union of seven sub-hypotheses, which together allow for each unique combination of tensor, vector, and scalar polarizations. The “TVS” sub-hypothesis, for example, assumes the simultaneous presence of all polarization modes, with a canonical energy-density spectrum of the form:

$$\Omega_{\text{TVS}}(f) = \Omega_0^T \left(\frac{f}{f_0}\right)^{\alpha_T} + \Omega_0^V \left(\frac{f}{f_0}\right)^{\alpha_V} + \Omega_0^S \left(\frac{f}{f_0}\right)^{\alpha_S}. \quad (\text{A2})$$

The “TS” sub-hypothesis, meanwhile, assumes only the existence of tensor and scalar modes:

$$\Omega_{\text{TS}}(f) = \Omega_0^T \left(\frac{f}{f_0}\right)^{\alpha_T} + \Omega_0^S \left(\frac{f}{f_0}\right)^{\alpha_S}. \quad (\text{A3})$$

In this fashion, we can construct seven unique sub-hypotheses: $\{\text{T,V,S,TV,TS,VS,TVS}\}$. The union of these

seven possibilities is the Signal hypothesis.

Non-standard polarization (NGR) – Analogous to the Signal hypothesis above, this is the union of the six sub-hypotheses $\{V, S, TV, TS, VS, TVS\}$ containing non-standard polarizations.

Tensor-polarization (GR) – We assume the stochastic background is present and purely-tensor polarized, with the energy-density spectrum

$$\Omega_{\text{GR}} = \Omega_0^T \left(\frac{f}{f_0} \right)^{\alpha_T}; \quad (\text{A4})$$

this hypothesis is identical the ‘‘T’’ signal sub-hypothesis above.

Odds Ratios

Here, we review the procedure for constructing odds $\mathcal{O}_{\text{N}}^{\text{SIG}}$ between Signal and Gaussian noise hypotheses, and odds $\mathcal{O}_{\text{GR}}^{\text{NGR}}$ between the NGR and GR hypotheses. As above, see Ref. [3] for further details.

The odds between two hypotheses \mathcal{M} and \mathcal{N} is the ratio of posterior probabilities for each hypothesis, given data d :

$$\begin{aligned} \mathcal{O}_{\mathcal{N}}^{\mathcal{M}} &= \frac{p(\mathcal{M}|d)}{p(\mathcal{N}|d)} \\ &= \mathcal{B}_{\mathcal{N}}^{\mathcal{M}} \frac{\pi(\mathcal{M})}{\pi(\mathcal{N})}, \end{aligned} \quad (\text{A5})$$

where $\mathcal{B}_{\mathcal{N}}^{\mathcal{M}}$ is the Bayes factor between the two hypotheses and $\pi(\mathcal{M})$ and $\pi(\mathcal{N})$ are the prior probabilities on \mathcal{M} and \mathcal{N} , respectively. The ratio $\pi(\mathcal{M})/\pi(\mathcal{N})$ is known as the prior odds.

To obtain $\mathcal{O}_{\text{N}}^{\text{SIG}}$, we first compute the Bayes factor $\mathcal{B}_{\text{N}}^{\mathcal{A}}$ between each Signal sub-hypothesis $\mathcal{A} \in \{T, V, S, \dots\}$ and the Noise hypothesis. Because each sub-hypothesis is independent, $\mathcal{O}_{\text{N}}^{\text{SIG}}$ is then just the sum

$$\begin{aligned} \mathcal{O}_{\text{N}}^{\text{SIG}} &= \sum_{\mathcal{A} \in \text{SIG}} \mathcal{O}_{\text{N}}^{\mathcal{A}} \\ &= \sum_{\mathcal{A} \in \text{SIG}} \mathcal{B}_{\text{N}}^{\mathcal{A}} \frac{\pi(\mathcal{A}|\text{SIG})\pi(\text{SIG})}{\pi(\text{N})}, \end{aligned} \quad (\text{A6})$$

where we have expanded $\pi(\mathcal{A}) = \pi(\mathcal{A}|\text{SIG})\pi(\text{SIG})$. We choose equal prior probabilities on the Signal and Noise hypotheses, such that $\pi(\text{SIG})/\pi(\text{N}) = 1$. Within the Signal hypothesis, we assign equal probabilities to each sub-hypothesis, giving $\pi(\mathcal{A}|\text{SIG}) = 1/7$.

The odds $\mathcal{O}_{\text{GR}}^{\text{NGR}}$ is analogously given by

$$\mathcal{O}_{\text{GR}}^{\text{NGR}} = \sum_{\mathcal{A} \in \text{NGR}} \mathcal{B}_{\text{GR}}^{\mathcal{A}} \frac{\pi(\mathcal{A}|\text{NGR})\pi(\text{NGR})}{\pi(\text{GR})}. \quad (\text{A7})$$

We set $\pi(\text{NGR})/\pi(\text{GR}) = 1$ and again choose equal prior probabilities for each sub-hypotheses within NGR, such that $\pi(\mathcal{A}|\text{NGR}) = 1/6$.

TABLE I. Bayes factors between each signal sub-hypothesis and the Gaussian noise hypothesis, as computed by `MultiNest`. These Bayes factors are combined following Eqs. (A6) and (A7) to obtain odds $\mathcal{O}_{\text{N}}^{\text{SIG}}$ between Signal and Gaussian noise hypotheses, and odds $\mathcal{O}_{\text{GR}}^{\text{NGR}}$ between NGR and GR hypotheses.

Hypothesis	$\ln \mathcal{B}_{\text{N}}^{\mathcal{A}}$
T	−0.33
V	−0.33
S	−0.31
TV	−0.66
TS	−0.65
VS	−0.65
TVS	−0.99

Our chosen prior odds between hypotheses are necessarily somewhat arbitrary, and different choices will yield different values of $\mathcal{O}_{\text{N}}^{\text{SIG}}$ and $\mathcal{O}_{\text{GR}}^{\text{NGR}}$. For completeness, Table I provides the Bayes factors between each signal sub-hypothesis and Gaussian noise. These Bayes factors allow readers to recompute odds $\mathcal{O}_{\text{N}}^{\text{SIG}}$ and $\mathcal{O}_{\text{GR}}^{\text{NGR}}$ using different choices of prior odds.

Calibration Uncertainty

The strain measured by LIGO-Hanford and LIGO-Livingston is not known perfectly, but is subject to non-zero calibration uncertainty. For imperfectly calibrated data, the cross-power measurements $\hat{C}(f)$ are not estimators of $\sum_A \gamma_A(f)\Omega^A(f)$, but rather of $\lambda \sum_A \gamma_A(f)\Omega^A(f)$, where λ is some multiplicative factor [5]. Perfect calibration would yield $\lambda = 1$, but in general λ is unknown. We include the calibration factor λ as an additional parameter in `MultiNest`, so that the likelihood function becomes

$$\begin{aligned} \mathcal{L}(\hat{C}(f)|\Omega_0^A, \alpha_A, \lambda) \\ \propto \prod_f \exp \left[- \frac{\left(\hat{C}(f) - \lambda \sum_A \gamma_A(f)\Omega_0^A(f/f_0)^{\alpha_A} \right)^2}{2\sigma^2(f)} \right], \end{aligned} \quad (\text{A8})$$

with $\hat{C}(f)$ and $\sigma^2(f)$ given by Eqs. (11) and (12) of Ref. [1], respectively.

We place a Gaussian prior on λ , centered at $\lambda = 1$:

$$\pi(\lambda) \propto \exp \left(- \frac{(\lambda - 1)^2}{2\epsilon^2} \right). \quad (\text{A9})$$

The standard deviation ϵ encapsulates the amplitude calibration uncertainty. Within the 20-1726 Hz frequency band, LIGO-Hanford and LIGO-Livingston have maximum estimated amplitude uncertainties of 4.8% and 5.4%, respectively [6]. These uncertainty estimates have been improved relative

to the the uncertainties previously adopted in Refs. [7–9]. For our analysis, we take $\epsilon = 0.072$, the quadrature sum of the Hanford and Livingston uncertainties [7]. All results are given after marginalization over λ .

In the above prescription we have made two simplifying assumptions. First, we have neglected phase calibration uncertainty, which is expected to be a sub-dominant source of uncertainty in the stochastic analysis [5, 6]. Secondly, although calibration uncertainties are frequency-dependent, for simplicity we adopt uniform amplitude uncertainties across all frequencies. Our quoted amplitude uncertainties are conservative, encompassing the largest calibration uncertainties in the stochastic sensitivity band [6, 7].

Detailed Parameter Estimation Results

In Ref. [1], we presented marginalized posteriors for the tensor, vector, and scalar background amplitudes under the “TVS” hypothesis. In Fig. 2 we show the full six-dimensional parameter estimation results obtained when choosing log-uniform amplitude priors. Diagonal subplots show marginalized posteriors on the amplitudes and slopes of each polarization, while the interior subplots show joint posteriors between each pair of parameters. The spectral index posteriors (not shown in Ref. [1]) are largely consistent with our choice of prior, but indicate a slight bias against large positive spectral indices. This reflects the fact that Advanced LIGO is most sensitive to backgrounds of large, positive slopes [3]. The non-detection of a stochastic background therefore constrains larger amplitudes to have small and/or negative spectral indices; see, for instance, the joint $\log \Omega_0^T - \alpha_T$ posterior in Fig. 2.

Figure 3, meanwhile, shows full parameter estimation results when alternatively assuming uniform amplitude priors. Here, the posterior preference towards small or negative spectral indices is far more pronounced. The joint 2D posteriors (e.g. $\Omega_0^T - \alpha_T$) again illustrate that large, positive slopes are preferentially ruled out in case of large background amplitudes.

As stated in Ref. [1], upper limits obtained under one hypothesis are not, in general, equal to those obtained under some different hypothesis. While we presented upper limits only for the TVS hypothesis, results from other hypotheses may be desired as well (the TS results, for instance, are best suited for comparison to predictions from scalar-tensor theories). In Tables II and III we have therefore listed the 95% credible upper limits corresponding to each signal sub-hypothesis, for both log-uniform and uniform amplitude priors. We have also listed 95% credible bounds on spectral indices for each choice of amplitude prior.

-
- [1] B. P. Abbott *et al.*, Phys. Rev. Lett. **120**, 201102 (2018).
 - [2] B. Allen and J. D. Romano, Phys. Rev. D **59**, 102001 (1999).
 - [3] T. Callister *et al.*, Phys. Rev. X **7**, 041058 (2017).
 - [4] D. Meacher *et al.*, Phys. Rev. D **92**, 063002 (2015).
 - [5] J. T. Whelan, E. L. Robinson, J. D. Romano, and E. H. Thrane, J. Phys. Conf. Ser. **484**, 012027 (2014).
 - [6] C. Cahillane *et al.*, Phys. Rev. D **96**, 102001 (2017).
 - [7] B. P. Abbott *et al.*, Phys. Rev. Lett. **118**, 121101 (2017).
 - [8] B. P. Abbott *et al.*, Phys. Rev. Lett. **118**, 121101 (2017), Online Supplement.
 - [9] B. P. Abbott *et al.*, Phys. Rev. Lett. **118**, 121102 (2017).

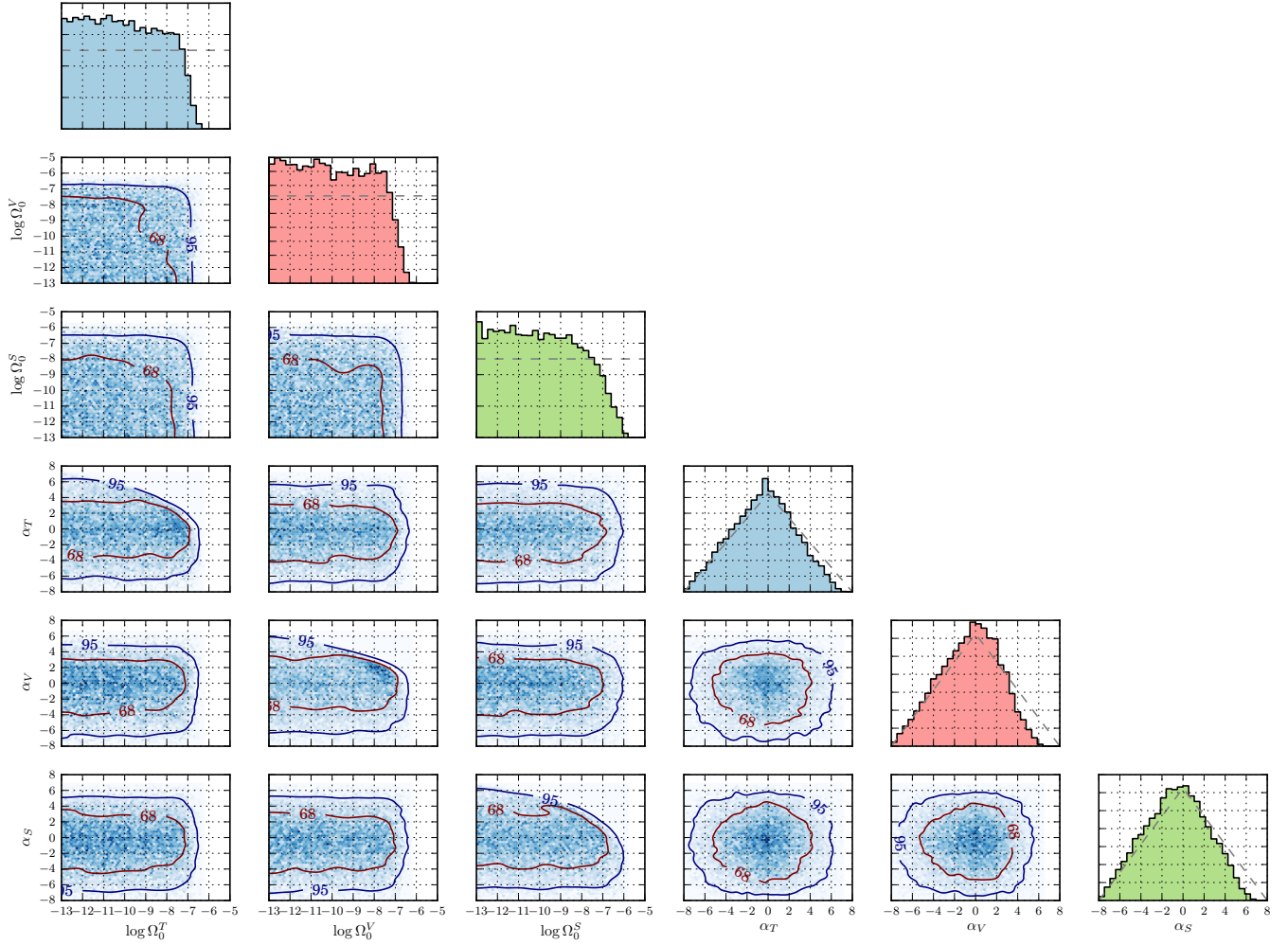


FIG. 2. Posterior probability distributions for the power-law amplitudes and slopes of tensor, vector, and scalar contributions to the stochastic background, assuming the TVS hypothesis and log-uniform amplitude priors. The subplots along the diagonal show marginalized posteriors for each parameter; dashed curves show the corresponding prior. The marginalized amplitude posteriors yield the 95% credible upper limits given in Table I. The remaining subplots, meanwhile, show the two-dimensional posteriors between each pair of parameters, as well as contours containing the central 68% and 95% posterior probability.

TABLE II. Parameter estimation results for each signal sub-hypothesis, obtained with log-uniform priors on the amplitude of each polarization component. Columns 2-4 give 95% credible upper limits on $\log \Omega_0^A$, and columns 5-7 show the corresponding limits on Ω_0^A for convenience. Columns 8-10, meanwhile, show the central 95% credible bounds on spectral indices α_A . The parameter estimation results for the TVS sub-hypothesis (final row) correspond to those given in Table I of the main text.

Hypothesis	$\log \Omega_0^{T,95\%}$	$\log \Omega_0^{V,95\%}$	$\log \Omega_0^{S,95\%}$	$\Omega_0^{T,95\%}$	$\Omega_0^{V,95\%}$	$\Omega_0^{S,95\%}$	α_T	α_V	α_S
T	-7.21	-	-	6.23×10^{-8}	-	-	$-0.4_{-5.9}^{+5.5}$	-	-
V	-	-7.16	-	-	6.96×10^{-8}	-	-	$-0.4_{-5.8}^{+4.9}$	-
S	-	-	-6.86	-	-	1.38×10^{-7}	-	-	$-0.5_{-5.8}^{+5.4}$
TV	-7.25	-7.16	-	5.56×10^{-8}	6.95×10^{-8}	-	$-0.4_{-5.9}^{+5.6}$	$-0.4_{-5.8}^{+4.8}$	-
TS	-7.25	-	-6.93	5.68×10^{-8}	-	1.18×10^{-7}	$-0.4_{-5.9}^{+5.5}$	-	$-0.5_{-5.8}^{+5.4}$
VS	-	-7.17	-6.90	-	6.74×10^{-8}	1.25×10^{-7}	-	$-0.4_{-5.9}^{+5.0}$	$-0.5_{-5.8}^{+5.4}$
TVS	-7.25	-7.20	-6.96	5.58×10^{-8}	6.35×10^{-8}	1.08×10^{-7}	$-0.4_{-5.9}^{+5.5}$	$-0.4_{-5.9}^{+4.8}$	$-0.6_{-5.8}^{+5.4}$

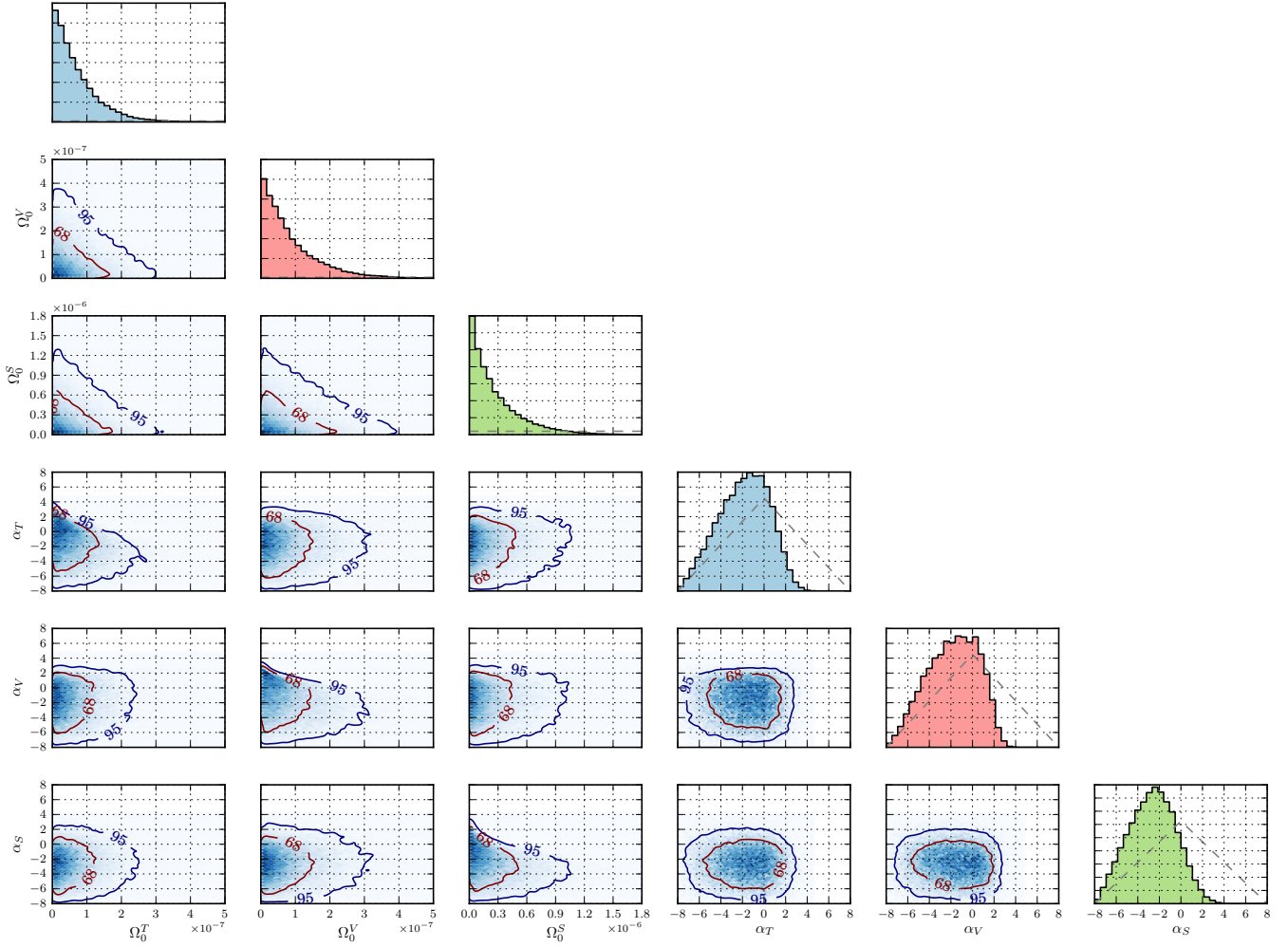


FIG. 3. As in Fig. 3, but assuming a uniform prior on background amplitudes. The marginalized amplitude posteriors yield the 95% credible upper limits given in Table I.

TABLE III. Parameter estimation results for each signal sub-hypothesis, obtained with uniform priors on the background amplitudes. Columns are defined as in Table II above. The parameter estimation results for the TVS sub-hypothesis (final row) correspond to those given in Table I of the main text.

Hypothesis	$\log \Omega_0^{T,95\%}$	$\log \Omega_0^{V,95\%}$	$\log \Omega_0^{S,95\%}$	$\Omega_0^{T,95\%}$	$\Omega_0^{V,95\%}$	$\Omega_0^{S,95\%}$	α_T	α_V	α_S
T	-6.60	-	-	2.53×10^{-7}	-	-	$-0.4^{+3.8}_{-4.7}$	-	-
V	-	-6.48	-	-	3.29×10^{-7}	-	-	$-1.5^{+3.3}_{-4.9}$	-
S	-	-	-5.97	-	-	1.08×10^{-6}	-	-	$-2.6^{+4.1}_{-4.0}$
TV	-6.66	-6.55	-	2.18×10^{-7}	2.85×10^{-7}	-	$-1.8^{+3.9}_{-4.7}$	$-1.7^{+3.6}_{-4.9}$	-
TS	-6.65	-	-6.03	2.23×10^{-7}	-	9.28×10^{-7}	$-1.7^{+3.8}_{-4.7}$	-	$-2.6^{+4.0}_{-4.1}$
VS	-	-6.53	-6.04	-	2.96×10^{-7}	9.21×10^{-7}	-	$-1.7^{+3.6}_{-4.7}$	$-2.8^{+4.1}_{-4.0}$
TVS	-6.70	-6.59	-6.07	2.02×10^{-7}	2.54×10^{-7}	8.44×10^{-7}	$-1.7^{+3.8}_{-4.8}$	$-1.7^{+3.7}_{-4.7}$	$-2.6^{+4.0}_{-4.1}$